Morphology and Interfacial Action of Nanocomposites Formed from Ethylene−Vinyl Acetate Copolymers and Organoclays

ARTICLE *in* THE JOURNAL OF PHYSICAL CHEMISTRY B · SEPTEMBER 2009

Impact Factor: 3.3 · DOI: 10.1021/jp903448t · Source: PubMed

Morphology and Interfacial Action of Nanocomposites Formed from Ethylene−Vinyl Acetate Copolymers and Organoclays

Qilu Zhang, Xiaoyan Ma,* Yifei Wang, and Kaichang Kou

Department of Applied Chemistry, School of Science, Northwestern Polytechnical University, Xi'an 710072, China

Received: April 15, 2009; Revised Manuscript Received: July 9, 2009

The effect of the polarity of modifier and polymer matrixes on the morphology and interfacial action of nanocomposites was studied by molecular dynamics (MD) and inverse gas chromatography (IGC) based on ethylene−vinyl acetate (EVA) /organic montmorillonite (OMMT), where vinyl acetate (VA) concentrations are 9.3 and 18 wt %, respectively. It is found that EVA with higher VA concentration displays a higher surface energy than that with lower VA concentration. Modifier with two long alkyl tails will lower the surface energy of montmorillonite (MMT) more effectively. Combined with transmission electron microscopy (TEM) photography of EVA/OMMT nanocomposites, it is found that the surface energies of organic montmorillonite and EVAs make great contributions to the dispersion of the OMMT in polymer matrixes. OMMT modified by two long alkyl tails displays weaker acid and base properties which will have a better interaction with EVAs through acid−base interaction. Molecular simulation (MD) proved that nonpolar interaction determines the binding between EVAs and organoclays, otherwise electrostatic interaction in polar polymer/organoclay systems. Binding energies were calculated by MD, and the results show stronger interaction between 20A (organoclay made from two long alkyl tails surfactant) and EVA. Interfacial action between filler and polymer matrix should be accountable for the mechanical properties of the nanocomposite.

1. Introduction

Polymer clay nanocomposites (PCNs) are currently receiving considerable attention for their good properties compared with polymers alone or conventional micro- and macro-composite materials because of clay's large aspect ratio.[1−3] The dispersion of filler and the degree of interfacial action between filler and matrixes directly affect the structure of their composites and make great a contribution to a series of properties of composite materials. In order to improve the dispersibility of fillers and enhance interaction between nanofillers and polymer matrixes, ammonium surfactants are usually used to modify clay and produce organoclays. The surfactant used may be primary, secondary, tertiary, and quaternary alkylammonium cations or some organic cations with functional groups. Organic cations in organoclay can enlarge interlayer *d*-spacing and lower the surface energy of inorganic host, resulting in better miscibility among components. Additionally, organic surfactant cations with functional groups can react with polymer matrixes, improving the strength of the interface between inorganic clay and polymer matrix. That means the interaction between organoclay and polymer matrixes plays a key role in forming clay nanocomposite.

The structure and properties of nanocomposites have been extensively studied to reveal how the structure of polymer and modifier affect the morphology and interfacial action. Previous studies[4−7] by many trailblazers show that polar polymer, like nylon, prefers to choose the organoclay made from one long tail surfactant, nonpolar polymer like polypropylene (PP) and polyethylene (PE) may favor to choose organoclay made from two long tails surfactant, and some polymer like thermoplastic polyurethane, styrene acrylonitrile copolymer (SAN), and polycarbonate (PC) may prefer to choose organoclay with some functional groups such as hydroxyl. Besides experimental studies, molecular simulation techniques have also been used to explore and characterize the atomic scale structure of nanocomposites based on different polymer matrixes and modifiers. Intercalated and exfoliated models of polymer nanocomposites based on polycaprolactone and functionalized montmorillonite (MMT) are built by Gardebien.[8,9] Molecular organization and interaction of MMT and polymer are studied for two systems. Binding energies of polymer/clay nanocomposites based on polypropylene, nylon-6, and nylon-6,6 have been calculated with several different quaternary ammonium salts as modifiers.[10−12] The results provided an overview influence of surfactant volume and functional groups on interfacial action in nylon-6/MMT nanocomposites. Balazs et al.[13] used numerical self-consistent field (SCF) calculations to investigate the interactions between two closely spaced surfaces and the surrounding polymer melt. Their conclusions gave a good explanation on the effect of polymer and surfactant on exfoliating the clay sheets.

To further understand the roles polymer and surfactant play, we[14] constructed three kinds of nanocomposite models composed of thermoplastic polyurethane (TPUR) and rectorite by molecular simulation, and it is found that organic rectorite (OREC) has a stronger interaction with TPUR than rectorite (REC). Meanwhile, we investigated the surface properties of the three kinds of clay and TPUR by inverse gas chromatography (IGC), and the results show that, through modification, surfactants lowered the surface energy of the REC and changed the clay surface from acid to alkaline, which will match the acidic surface of TPUR by acid−base interaction. Finally, we proposed that there is some relationship between our data obtained and the morphology and mechanical properties of PCNs; i.e., the decreased dispersive energy of REC can improve their dispersibility in low surface energy TPUR and form a

* Corresponding author. Phone: +86 2988431676. Fax: +86 2988491826. E-mail: m_xiao_yana@nwpu.edu.cn.

10.1021/jp903448t CCC: $40.75
Published on Web 08/13/2009

TABLE 1: Organoclays Used in This Study

Organoclay designation	SCP designation	Designation for short	chemical structure of Surfactant cation
$M_2(HT)_2$	Cloisite 20A	20A	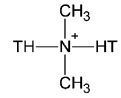
$(HE)_2M1T_1$	Cloisite 30B	30B	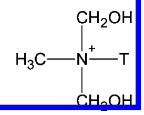

uniform morphology; and a matched acid−base action can enhance the interaction of filler and polymer matrix, resulting in a higher interfacial strength and consequently better mechanical properties. However, we do not exactly know the role polymer plays, e.g., how the polarity of polymer affects the morphology and properties of nanocomposite. For this consideration, we build structure models of two kinds of organic montmorillonite (OMMT) and two kinds of ethylene−vinyl acetate (EVA) copolymers with different vinyl acetate (VA) concentrations using the technique of molecular simulation, and calculate the interaction energy between OMMTs and polymers. Also, we report IGC measurements of the surface properties of OMMTs and EVAs to analyze the compatibility of surface properties, i.e., their surface energy and acid−base properties.

2. Experimental and Modeling

2.1. Materials. The EVA used in this study was produced by DuPont with VA concentrations of 9.3% (EVA9.3, trade name is Elvax 760Q) and 18% (EVA18, trade name is Elvax 460), respectively.

Organoclays, generously donated by Southern Clay Products, Inc., were formed by cation exchange between sodium montmorillonite (CEC = 92 mequiv/100 g of clay) and various quaternary ammonium salts. Some frequently used abbreviations are employed here to represent the substituents on the ammonium cation, e.g., M for methyl and HE for 2-hydroxy-ethyl, while T and HT represent long alkyl chains from natural tallow oil and hydrogenated tallow, respectively (Table 1). These organoclays were selected to explore the effects of the ammonium surfactant structure on the dispersion of the clay particles in different EVA copolymer matrixes.

Nonpolar solvents (hexane, heptane, octane, and nonane) and polar solvents (chloroform, ethyl acetate, acetone, tetrahydrofuran (THF), dioxane, and diethyl ether), provided by Shanghai Chemical Reagent Company of China, were used as probes. All of these solvents are of analytical grade and used without further purification.

2.2. IGC Analysis. The mineral stationary phases were prepared by compacting OMMT grinding and sieving to a particle size of 180−250 mm, respectively. The stationary phases were packed into 600 mm × 3.0 mm stainless steel columns and conditioned at 150 °C under nitrogen for 24 h prior to use.

The polymer stationary phases were prepared by the support for the preparation of chromatographic columns, and diatomite was coated with EVA solution according to the soaking method of Al-Saigh and Munk,[15] then dried at room temperature to constant weight in a vacuum oven to obtain 10 wt % polymer coated based on the weight of support, and sieved to a particle size of 180−250 mm. The four stationary phases were packed into 600 mm × 3.0 mm stainless steel columns and conditioned at 100 °C under nitrogen for 24 h prior to use.

IGC analysis was performed on a GC7890II gas chromatograph (Tianmei Apparatus Company in Shanghai, China) equipped with a flame ionization detector. Dried nitrogen was used as a carrier gas and flow rates were measured using a calibrated soap bubble flowmeter. A small quantity of solvent was injected manually with a 0.1 mL Hamilton syringe. Retention times were recorded and processed by the N2000 chromatography workstation (Zhejiang University, China). Methane gas was used as a noninteracting marker to correct the dead volume in the column. Each value reported is the result of at least three elutions. The usual checks were carried out to ensure that results were recorded at infinite dilution.

3. Methodology of Molecular Simulation

Montmorillonite is an aluminosilicate made up of one aluminate octahedral sheet sandwiched between two silicate tetrahedral sheets. Isomorphous substitution of metal ions in the crystal lattice by cations of lower charge causes a net permanent negative charge that is balanced by cations in the interlayer space. The clay platelet of MMT has x and y dimensions of 31.2 Å by 27.6 Å, respectively, and bears a negative charge of 11 e, which results from the substitutions of Si atoms by Al atoms and Al atoms in octahedral positions by Mg atoms.

The d-space of the intercalated 20A nanocomposite is 2.57 nm according to its WAXD data.[16] In the interlayer, 11 surfactants were inserted to displace free cations, and the organic phase also consists of four "macromolecules" of EVAs. Accordingly, the total interlayer density of the organic phase has become 1.04 g·cm^{-3}, which is appropriate in the case of nanocomposite.[10] For 30B, the interlayer (the d-space is 1.82 nm by WAXD data[16]) is too narrow to add the 11 surfactants (the density is about 1.2 g·cm^{-3} in the interlayer). The abnormal phenomena of the low d-spacing have been widely reported for olefin-polymer-based nanocomposites.[16−19] In this paper, the parameters for 30B are chosen arbitrarily by keeping the same organic phase density, number of surfactants, and "macromolecules" with 20A; thus, the d-spacing is calculated to be 2.09 nm.

The structural formula of EVA contains repeated ethylene and vinyl acetate as follows:

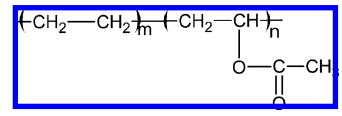

When $m = 30$ and $n = 1$, the VA concentration will come to approximate 9.3 wt %, and when $m = 28$ and $n = 4$, the VA concentration is about 18 wt %. In this paper, we constructed two models of EVAs to study their interaction with 20A and 30B. The charges of EVAs and the modifier, $M_2(HT)_2$ and $(HE)_2M_1T_1$, were derived from their electrostatic potential calculated at the HF/6-31G(d) level of theory (NBO method as implemented in Gaussian 03, revision B.01).[20] Some of the charges are illustrated in Figure 1. It is unhoped for that the nitrogen atom bears a negative charge other than the positive we expected. It is well-known that nitrogen has a higher electronegativity than carbon, so in the covalent bond between nitrogen and carbon, the electron cloud will prefer to approach the atom of nitrogen. The positive charge of nitrogen delocalizes

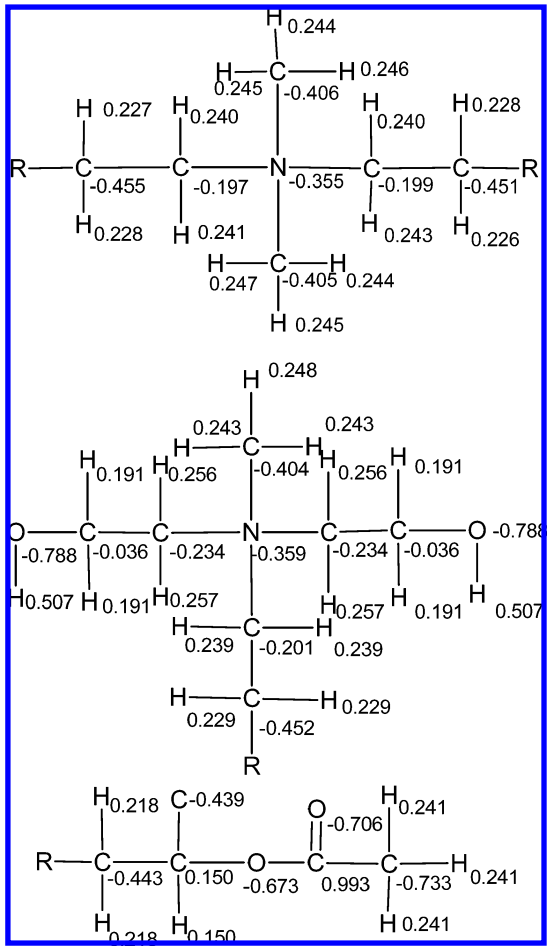

Figure 1. Atomic charges (in atomic units e) for selected atoms of 20A, 30B, and EVA (segment of ester linkage).

over other atoms in the molecule, which is in agreement with the conclusion we obtained before.[14] In our study, the two methylene groups and two methyl groups conjoin with the nitrogen atom to bear a total charge of 0.873, which means that it is the "head" of the surfactant, not the nitrogen atom, that displays the positive charge. Gardebien et al.[21] found a similar result on the $(HE)_2M_1T_1$ molecule. They reported a low positive charge of 0.05 by the CHELPG method in the Gaussian 98 package, and 70% of the excess positive charge is delocalized over the three methylene groups and the methyl group bound to the nitrogen atom.

The universal force field (UFF)[22] has been used throughout the whole simulation. For molecular dynamics (MD), the Ewald summation method was used for the treatment of electrostatic interactions. For van der Waals interactions, the Lennard-Jones potential was driven smoothly to zero for distances between 8.0 and 8.5 Å. Three-dimensional periodic boundary conditions were imposed to avoid boundary artifacts. All simulations were performed in the NVT ensemble and were coupled to a Nosé−Hoover thermostat[23−25] to maintain the temperature. Positions of atoms of the clay were maintained fixed throughout all of the simulations.

The initial configurations of OMMT and nanocomposites may be obtained by placing an organic molecule parallel or perpendicular to the interlayer surface from the literature.[21,26] However, in this study, modifiers and macromolecules were randomly placed between platelets to avoid the influence of initial structure on final configuration. For the generation of the final structure, three initial models were built and sent to performed a 1000 ps molecular dynamic (MD) running on 1000 K. From the generated sets of configurations, we then extracted the three configurations according to two criteria related to their potential energy: the configurations were selected on the basis of both the lowest nonbond energy and the lowest possible total torsion energy. The bond and angle energetic contributions were discarded from the selection criteria for two reasons. First, their large contributions to the potential energy may bias the selection toward, for example, configurations corresponding to high nonbond energy terms and accidentally low bond and angle potential terms. Second, the successive values of the bond and angle energy contributions cannot be directly related to the configuration changes of the whole organic phase.[9] For the extracted configurations, a 3000 ps MD simulation at 1000 K was performed for each structure. The high temperature was adopted to get a quick equilibrium; finally, the obtained system was sent to a MD simulation for 1000 ps at 293 K. The final configuration was used to calculate properties of nanocomposites.

4. Results and Discussion

4.1. IGC Analysis. Inverse gas chromatography (IGC) has been widely used in investigating surface properties of polymers. By IGC, the dispersive and Lewis acid−base interaction between the fixed phase and the flow phase in a column can be tested under special conditions, and the total surface energy can be written as the sum of the following two items:[27]

$$\gamma_S = \gamma_S^D + \gamma_S^{SD} \tag{1}$$

where γ_S^D and γ_S^{SD} are dispersive and specific contributions, respectively. In this study, dispersive and specific contributions were characterized for all of the samples using the method of IGC.

4.1.1. The Dispersion Component of Surface Free Energy. In IGC, at infinite dilution, the dispersive component of surface energy can be characterized by injecting a homologous series of *n*-alkanes into the column containing the polymer.

The primary measurement in IGC is the specific retention volume, V_g, which can be calculated from the following equation:[28]

$$V_g = Fj\frac{(t_R - t_M)}{m}\left(\frac{p_0 - p_w}{p_0}\right)\left(\frac{T}{T_{meter}}\right) \tag{2}$$

where F is the carrier gas flow rate, t_R is the retention time, t_M is the retention time of a nonadsorbing marker (air), p_0 is the outlet column pressure, p_w is the vapor pressure of water at the flowmeter temperature, T_{meter} and T are the ambient and column temperature, respectively, m is the mass of adsorbent, and j is the James−Martin compressibility factor.

The free energy of adsorption ΔG_a of *n*-alkanes is given by

$$\Delta G_a = RT \ln V_n + C \tag{3}$$

where R is the ideal gas constant, T the absolute temperature, and C a constant depending on the reference state of adsorption. In the case of *n*-alkanes, ΔG_a is equal to the free energy of adsorption corresponding to dispersive interactions only.

Since ΔG_a or $RT \ln V_n$ varies linearly with the number of carbon atoms of *n*-alkanes, it becomes possible to define an incremental value, ΔG_{CH_2}, which no longer depends on the

arbitrary choice of the standard reference state of the adsorbed alkane. That is,[29]

$$\Delta G_{CH_2} = -RT \ln(V_{g,n}/V_{g,n+1}) \quad (4)$$

which thus allows calculation of the dispersive component γ_S^D of the surface free energy as[27]

$$\gamma_s^D = (\Delta G_{CH_2}/Na_{CH_2})^2/(4\gamma_{CH_2}) \quad (5)$$

where $V_{g,n}$ and $V_{g,n+1}$ are the specific retention volume of alkanes having n and $n + 1$ atoms of carbon, respectively; N is Avogadro's number; a_{CH_2} is the area of a $-CH_2-$ group; and γ_{CH_2} is the surface energy of a surface made of CH_2 groups.

As the column temperature has a relationship with the specific retention volume of alkanes, we choose a different column temperature that can gain good symmetrical and nondelayed absorb curves. In this paper, samples were tested from 40 to 100 °C. The plots of $-RT \ln V_g$ versus temperature for a series of alkane probes on the materials are exemplified for the samples, as shown in Figure 2.

It could be seen from Figure 2 that all of the plots exhibit a linear relationship within the experimental temperature range, suggesting that the equilibrium between solvents and samples had been achieved. This indicated that V_g values were amenable for thermodynamic analysis. According to eq 5, γ_s^D values of the samples can be calculated, as shown in Figure 3.

These results indicate that surface dispersive energies of all samples reduce as the temperature increases, and EVA18 possesses a higher energy than EVA9.3, which should be due to its higher VA concentration. Furthermore, we found that the γ_s^D value of EVA18 was closest to that of 20A. A similar situation presented when we calculated the surface energy of thermoplastic polyurethane and two kinds of organic rectorite.[14] Combined with transmission electron microscopy (TEM) photographs of the obtained nanocomposites, we found that filler with a surface energy close to that of the polymer matrix would lead to good dispersion in the nanocomposite. TEM figures (nanocomposites containing both 5[16] and 1 wt % MMT) and results of particle analysis [16](based on TEM photographs of nanocomposites containing 5 wt % MMT) of EVA/OMMT, shown in Figures 4 and 5 and Table 2, illustrate that OMMT, both 20A and 30B, in EVA18/OMMT (EVA18/20A and EVA18/30B) displays better dispersion than OMMT in EVA9.3/OMMT (EVA9.3/20A and EVA9.3/30B), and in polymer with the special concentration of EVA, 20A modified nanocomposites exhibit better dispersion than 30B. Taking into account the dispersive data from IGC, it is concluded that the more close dispersive energies two components possess, the better morphology nanocomposites display. The result agrees well with what we found before.[14] However, as a puny polar polymer, EVA possesses a much lower surface dispersive energy than organoclay made from one long tail surfactant like 30B. This may give an explanation for why nonpolar polymers like PP and PE favor to choose organoclay made from two long tails surfactant.

4.1.2. Lewis Acid−Base Interactions. A comprehensive insight into the Lewis acid−base surface interactions of filler and polymer matrixes can provide better understanding of influence on the physical and mechanical properties of nanocomposites, which is of great importance for choosing surfactant in modifying plastics with organic clay. IGC is widely used in characterizing Lewis acid−base interactions between two matters, and good results can be expected.[30−33]

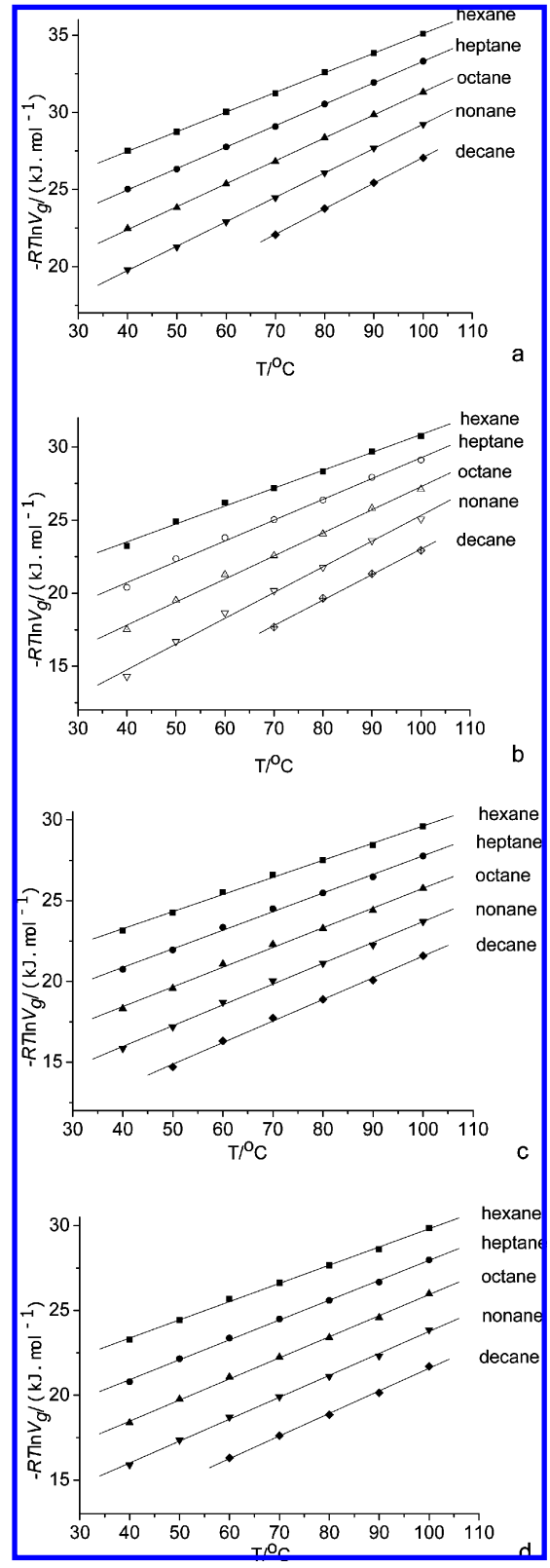

Figure 2. Plots of $-RT \ln V_g$ versus temperature for alkane probes on (a)20A, (b)30B, (c) EVA9.3, and (d) EVA18.

According to Brookman and Sawyer, the contribution of specific interactions to the free energy of adsorption or polarization free energy, ΔG_a^{AB}, may be described as the difference between specific polar adsorbate and imaginary n-alkane that possesses the same saturated vapor pressure. ΔG_a^{AB} can be

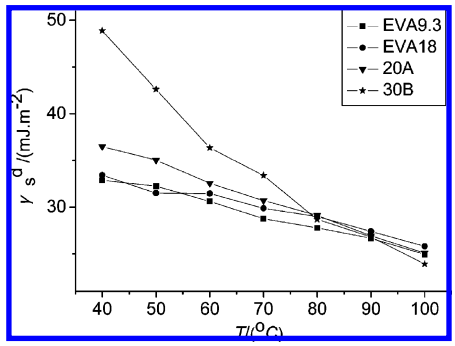

Figure 3. Variation of the dispersion energy of 20A, 30B, EVA-9.3, and EVA-18.

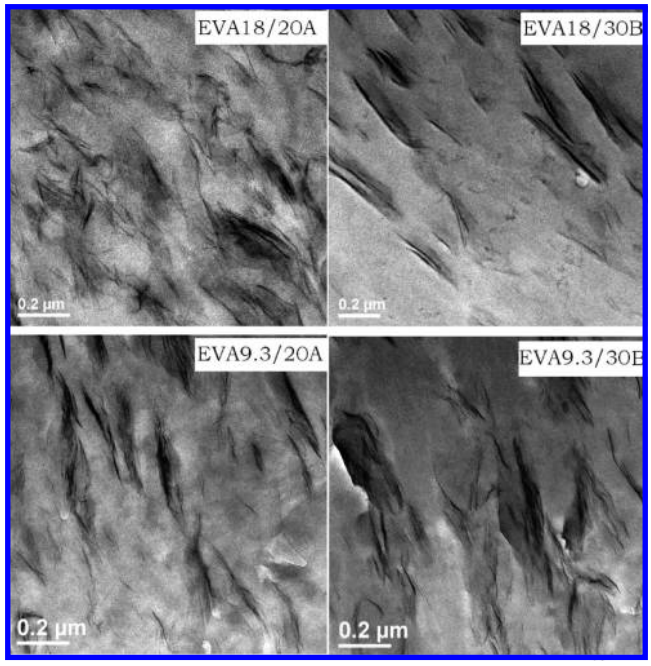

Figure 4. TEM of EVA/OMMT nanocomposites containing 5 wt % MMT.[16]

calculated by the following equation:[34]

$$-\Delta G_a^{AB} = RT \ln V_g^0 - RT \ln V_g^{ref} \quad (6)$$

where V_g^0 is the specific retention volume of a polar probe and V_g^{ref} is the retention volume of the hypothetical alkane that possesses the same saturated vapor pressure as the corresponding polar probe. Flour and Papirer suggested that a plot of $RT \ln V_g^0$ as a function of the logarithm saturated vapor pressure (lg P_0) of the alkane probe should be a straight line, which could act as a standard. The results for polar probes always deviate from the reference line to some extent. Figure 6 displayed ΔG_a^{AB} versus the logarithm of saturated vapor pressure, lg P_0, plots for EVA9.3 and EVA18 samples.

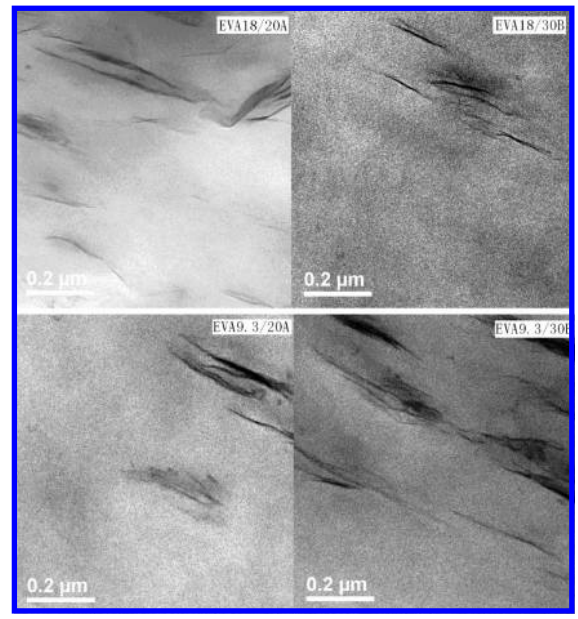

Figure 5. TEM of EVA/OMMT nanocomposites containing 1 wt % MMT.

Acidic probes, chloroform, and tetrachloromethane in Figure 6, exhibited significant deviations relative to the reference line for EVA9.3 and EVA18, indicating different alkalescence of EVAs. On the other hand, THF, the basic probe, also presented a stronger specific interaction with EVAs, indicating different acidic active sites on the surfaces of these polymers. To further understand the acid−base properties of EVAs and OMMTs, ΔG_a^{AB} was calculated, which indicates the polarity of polymers quantificationally. ΔG_a^{AB} values of the polar probes are illustrated in Table 3. The acidic chloroform displays larger polarization free energy with EVA18, indicating a larger interaction between chloroform and the polymer. However, THF with strong alkalescence interacted weakly with EVA18 but strongly with EVA9.3. In other words, EVA9.3 has a higher acidity and lower alkalescence than EVA18 due to the different concentrations of VA.

The acid constant (K_a) and base constant (K_d), which usually describe the ability of a polymer surface to act as an electron acceptor and donor, are related to the enthalpy of adsorption of polar probes, $-\Delta H_a^{AB}$, by the following equation based on the Saint and Papirer approach:

$$-\Delta H_a^{AB} = DNK_a + ANK_d \quad (7)$$

where DN[35] and AN[36] are the donor and acceptor values of polar probes, respectively. $-\Delta H_a^{AB}$ can be calculated by the following equation:

TABLE 2: Results of Particle Analysis of Nanocomposites Containing 5 wt % MMT (*l* and *t* Represent the Particle Length and Thickness of MMT)[16]

organoclay	vinyl acetate (wt %)	total number of particles	number average aspect ratio $\langle l/t \rangle_n$	$\bar{l}_n/\bar{t}_n$	weight average aspect ratio $\langle l/t \rangle_w$	$\bar{l}_w/\bar{t}_w$
$M_2(HT)_2$	9.3	265	26.5	18.5	37.7	14.5
	18	563	31.5	21.1	43.4	15.7
$(HE)_2M_1T_1$	9.3	477	16.2	12.9	24.8	10.8
	18	495	20.6	16.5	28.6	10.6

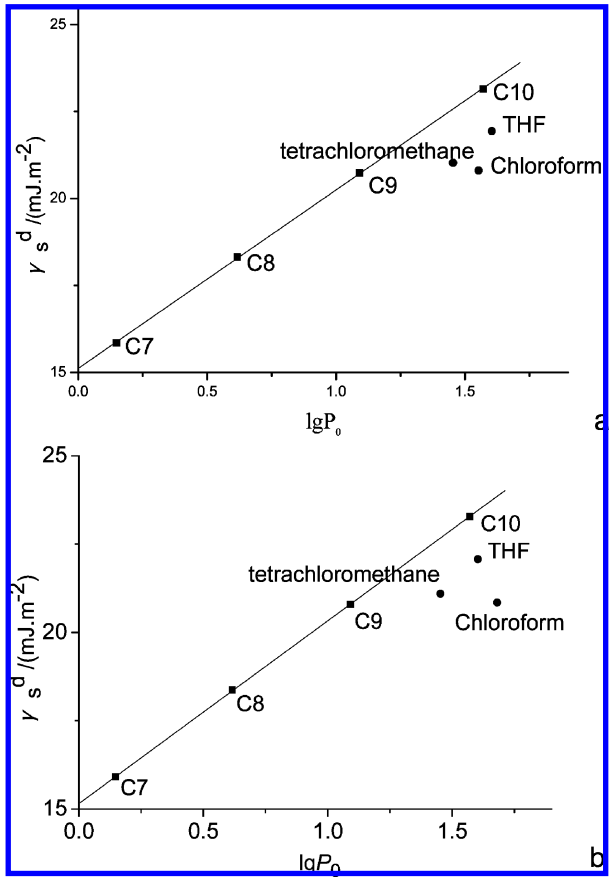

Figure 6. Plots of $-RT \ln V_g$ vs lg P_0 of polar and apolar probes on (a) EVA9.3 and (b) EVA18 at 313 K.

TABLE 3: ΔG_a^{AB} Values of the Polar Probes on EVA and OMMT at 60 °C (mJ·m^{-2})

stationary phases	chloroform	tetrachloromethane	THF	acetone
EVA9.3	2.36	1.55	1.35	
EVA18	2.68	1.56	1.38	
30B	4.57	1.94	8.69	
20A			5.89	8.41

$$\Delta G_a^{AB} = \Delta H_a^{AB} + \Delta S_a^{AB} T \quad (8)$$

where ΔS_a^{AB} is the entropy of adsorption of the polar probe. $-\Delta H_a^{AB}$ can be obtained from slopes of the plots of $\Delta G_a^{AB}/T$ as a function of $1/T$. K_a and K_d could be calculated from eq 7, by a two-variable linear regression model, and summarized in Table 4. EVA9.3 and EVA18 show very low acid−base character by the data, and the difference between the two systems was considered to be an error for their low values. 20A exhibits lower acidity and alkalescence than 30B because of the puny polarity of its modifier. In the previous study by this laboratory,[14] we found that weak basic properties of filler may have a good interaction with polymer matrix with weak acidic surface properties. Hence, the data in Table 4 indicate a better interfacial action for the EVA/20A system than 30B modified nanocomposites. Further discussion with respect to interfacial action and mechanical properties of nanocomposites will be performed in section 4.2.

4.2. Molecular Simulation Analysis. For a further understanding of the interaction between polymer and OMMT, and also surfactant and MMT, MD was performed to analyze how the polarity of modifier and polymer influences the morphology and properties of nanocomposite.

TABLE 4: Data of Acid−Base Characteristics of EVA9.3, EVA18, 20A, and 30B

sample	K_a	K_d
EVA9.3	0.09	0.06
EVA18	0.07	0.09
30B	0.54	1.41
20A	0.40	1.23

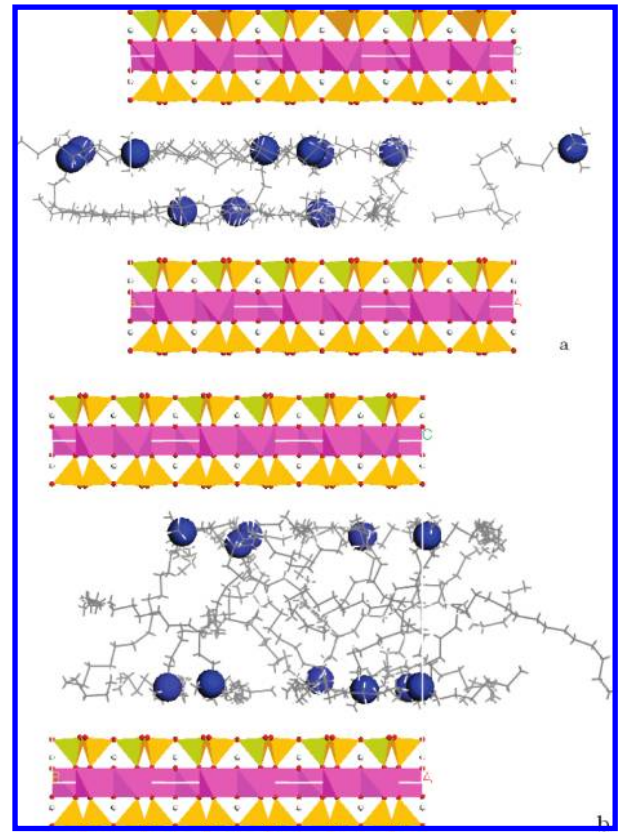

Figure 7. Snapshot of the simulations of the 20A and 30B models. The clay layer is represented by one octahedral sheet sandwiched between two tetrahedral sheets. The nitrogen of the surfactants is represented with spheres, and the other atoms, with lines. From the figure, we can see that heads, segments around nitrogen, are stuck to the surface of the MMT sheet by electrostatic action.

The final structures of OMMTs and nanocomposites are shown in Figures 7 and 8. As expected, all of the charged heads of the surfactants stuck to the surface, while their hydrophobic tails are either adsorbed on the surface or extended away from the surface. Figure 9 shows the distribution of organic modifiers in the interlayer clay sheet in OMMT (in view onto the platelet). For clarity, both clay sheets and polymer were taken off from the actual snapshot. It can be seen from Figure 9 that $M_2(HT)_2$ covers more surface of the clay sheet than $(HE)_2M_1T_1$, which should be a key reason for the lower surface dispersive energy of 20A.

The binding energy $E_{EVA18/20A}$ can be calculated according to the following equation:

$$E_{EVA18/20A} = E_{EVA18} + E_{20A} - E_{total} \quad (9)$$

in which $E_{EVA18/20A}$ is the binding energy between EVA18 and 20A; E_{EVA18} and E_{20A} represent the corresponding energy of EVA18 and 20A in the optimized conformation of the composite, respectively; and E_{total} is the total energy of the nanocomposite. In order to compute the binding energy between

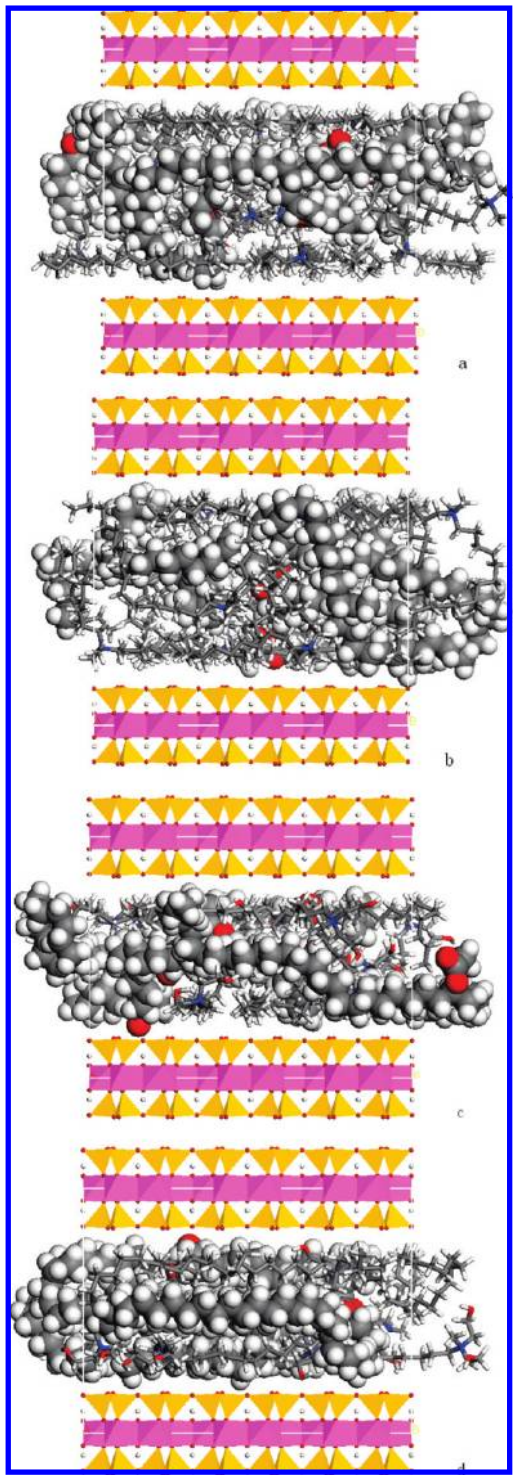

Figure 8. Snapshot of the simulations of the (a) EVA-18/20A, (b) EVA-9.3/20A, (c) EVA-18/30B, and (d) EVA-9.3/30B nanocomposite models. The clay layer is represented by one octahedral sheet sandwiched between two tetrahedral sheets. The surfactants are represented with sticks, and the PCL chains, with spheres.

EVA18 and 20A, the model after molecular dynamic simulation of the nanocomposite (shown in Figure 6b) should be constructed to calculate E_{total}. The corresponding energy E_{EVA18} was calculated from the optimized conformation of the composite by removing surfactant molecules and clay platelets without further minimization, and E_{20A} was obtained by the same way after removing all of the macromolecules out from the optimized conformation of nanocomposite. Similarly, the binding energies

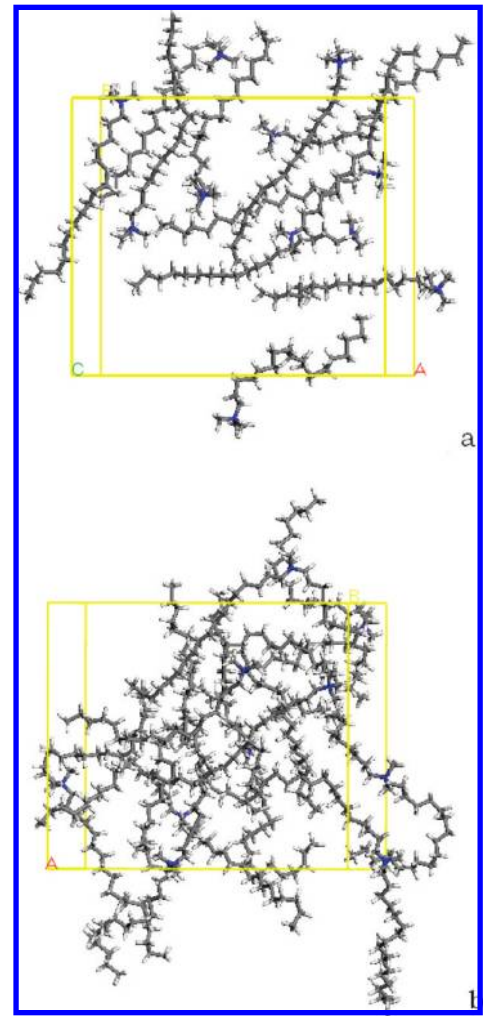

Figure 9. Distribution of organic modifiers in the interlayer clay sheet in OMMT (on view onto the platelet).

TABLE 5: van der Waals, Electrostatic, and Total Contributions to the Binding Energies (in kcal/mol) between "Macromolecules" and OMMT in Nanocomposites

system	EVA18/20A	EVA9.3/20A	EVA18/30B	EVA9.3/30B
total	599	487	484	397
van der Waals	619	594	473	470
electrostatic	−20	−107	11	−74

between "macromolecules" and OMMT in other systems of nanocomposites were calculated and reported in Table 5.

The total binding energies of the four systems are mainly contributed by van der Waals energies, which means, in EVA/OMMT nanocomposites, nonpolar (van der Waals force is mainly contributed by dispersive force) interaction determines the binding between polymer and organoclay. It can also be found from Table 5 that EVA, with different VA concentrations, has a more stable binding between polymer and OMMT in EVA/20A naocomposite than in the EVA/30B system (in agreement with the conclusion obtained in section 4.1.2). For the two kinds of EVA-based organoclays, a higher value of binding energies always displays in systems based on EVA18 because of both its higher van der Waals energy and electrostatic energy. However, increasing electrostatic energy plays a key role in increasing the total binding energy (for EVA/20A systems, the increases of van der Waals energy and electrostatic energy are 25 and 87 kcal/mol, respectively, when the VA concentration

increases, and for EVA/30B systems, the increases are 3 and 85 kcal/mol, respectively).

High interfacial binding energy between clay and polymer should be responsible for high mechanical properties of nanocomposites. The moduli of EVA18/20A, EVA18/30B, EVA9.3/20A, and EVA9.3/30B nanocomposites are reported in ref 16. For EVA18/20A and EVA18/30B, the nanocomposite modified by 20A possesses a higher module, which agrees with results of binding energy and acid−base interaction analysis (EVA18/20A has a stronger interfacial action than EVA18/30B), and for EVA9.3/20A and EVA9.3/30B systems, a similar conclusion can be obtained.

5. Conclusions

The methods of IGC and MD have been employed to analyze the effect of the polarity of the modifier and polymer matrix on the morphology and interfacial action of nanocomposites. Polymer and modifier polarity should be responsible for their surface dispersive energies, which will further affect nanocomposite morphology. The more close dispersive energies two components possess, the better morphology nanocomposites display. What is more, surfactant with two long alkyl tails covers more surface of a clay sheet than a one-tail surfactant, which will further lower the dispersive energy of MMT. The polarity of the modifier and polymer could also affect the interfacial action of the nanocomposite. 20A has weaker acid−base properties than 30B because its modifier, $M_2(HT)_2$, displays weaker polarity, and leads to better interfacial action than the EVA/30B system. A MD study revealed that, in EVA/OMMT nanocomposites, nonpolar interaction determines the binding between polymer and organoclay. EVA, with different VA concentrations, has a more stable binding between polymer and OMMT in EVA/20A nanocomposites than in EVA/30B systems. For the two kinds of organoclays, a higher value of binding energies always displays in the system based on EVA18, and increasing the electrostatic energy plays a key role in increasing the total binding energy. Stronger interaction between organoclay and polymer matrix will lead to a higher module of nanocomposite in certain polymer-based nanocomposites.

Acknowledgment. Part of the calculations were performed in the High Performance Computing Center of the Northwestern Polytechnical University. Supported by National Science Foundation of China (20674062) and New Century Excellent Talents in University (NCET-06-0880).

References and Notes

(1) Cui, L. L.; Ma, X. Y.; Paul, D. R. *Polymer* **2007**, *48*, 6325.
(2) Jeon, K.; Lumata, L.; Tokumoto, T.; Steven, E.; Brooks, J.; Alamo, R. G. *Polymer* **2007**, *48*, 4751.
(3) Dennis, H. R.; Hunter, D. L.; Chang, D.; Kim, S.; White, J. L.; Cho, J. W.; et al. *Polymer* **2001**, *42*, 9513.
(4) Fornes, T. D.; Hunter, D. L.; Paul, D. R. *Macromolecules* **2004**, *37*, 1793.
(5) Bae, W. J.; Kim, K. H.; Jo, W. H.; Park, Y. H. *Macromolecules* **2004**, *37*, 9850.
(6) Barber, G. D.; Calhoun, B. H.; Moore, R. B. *Polymer* **2005**, *46*, 6706.
(7) Chen, B.; Evans, J. R. G. *Macromolecules* **2006**, *39*, 747.
(8) Gardebien, F.; Gaudel-Siri, A.; Brédas, J. L.; Lazzaroni, R. *J. Phys. Chem. B* **2004**, *108*, 10678.
(9) Gardebien, F.; Brédas, J. L.; Lazzaroni, R. *J. Phys. Chem. B* **2005**, *109*, 12287.
(10) Fermeglia, M.; Ferrone, M.; Pricl, S. *Fluid Phase Equilib.* **2003**, *212*, 315.
(11) Toth, R.; Coslanich, A.; Ferrone, M.; Fermeglia, M.; Pricl, S.; Miertus, S.; Chiellini, E. *Polymer* **2004**, *45*, 8075.
(12) Tanaka, Genzo.; Goettler, L. A. *Polymer* **2002**, *43*, 541.
(13) Balazs, A. C.; Singh, C; Zhulina, E. *Macromolecules* **1998**, *31*, 8370.
(14) Ma, X. Y.; Qu, X. H.; Zhang, Q. L.; Chen, F. *Polymer* **2008**, *49*, 3590.
(15) Al-Saigh, Z. Y.; Munk, P. *Macromolecules* **1984**, *17*, 803.
(16) Cui, L. L.; Ma, X. Y.; Paul, D. R. *Polymer* **2007**, *48*, 6325.
(17) Shah, R. K.; Hunter, D. L.; Paul, D. R. *Polymer* **2005**, *46*, 2646.
(18) Hotta, S.; Paul, D. R. *Polymer* **2004**, *45*, 7639.
(19) Shah, R. K.; Paul, D. R. *Polymer* **2006**, *47*, 4075.
(20) Frisch, M. J. ; Trucks, G. W.; Schlegel, H. B.; Scuseria, G. E.; Robb, M. A.; Cheeseman, J. R. Montgomery, J. A. Vreven, J. T.; Kudin, K. N.; Burant, J. C.; Millam, J. M.; Iyengar, S. S.; Tomasi, J.; Barone, V.; Mennucci, B.; Cossi, M.; Scalmani, G.; Rega, N.; Petersson, G. A.; Nakatsuji, H.; Hada, M.; Ehara, M.; Toyota, K.; Fukuda, R.; Hasegawa, J.; Ishida, M.; Nakajima, T.; Honda, Y.; Kitao, O.; Nakai, H.; Klene, M.; Li, X.; Knox, J. E.; Hratchian, H. P.; Cross, J. B.; Adamo, C.; Jaramillo, J.; Gomperts, R.; Stratmann, R. E.; Yazyev, O.; Austin, A. J.; Cammi, R.; Pomelli, C.; Ochterski, J. W.; Ayala, P. Y.; Morokuma, K.; Voth, G. A.; Salvador, P.; Dannenberg, J. J.; Zakrzewski, V. G.; Dapprich, S.; Daniels, A. D.; Strain, M. C.; Farkas, O.; Malick, D. K.; Rabuck, A. D.; Raghavachari, K.; Foresman, J. B.; Ortiz, J. V.; Cui, Q.; Baboul, A. G.; Clifford, S.; Cioslowski, J.; Stefanov, B. B.; Liu, G.; Liashenko, A.; Piskorz, P.; Komaromi, I.; Martin, R. L.; Fox, D. J.; Keith, T.; Al-Laham, M. A.; Peng, C. Y.; Nanayakkara, A.; Challacombe, M.; Gill, P. M. W.; Johnson, B.; Chen, W.; Wong, M. W.; Gonzalez, C.; Pople, J. A. *Gaussian 03*; Gaussian, Inc.: Pittsburgh, PA, 2003.
(21) Gardebien, F.; Brédas, J. L.; Lazzaroni, R. *J. Phys. Chem. B* **2005**, *109*, 12287.
(22) Rappe, A. K.; Casewit, C. J.; Colwell, K. S.; Goddard, W. A.; Skiff, W. M. *J. Am. Chem. Soc.* **1992**, *114*, 10024.
(23) Nose', S.; Klein, M. *Mol. Phys.* **1983**, *50*, 1055.
(24) Nose', S. *J. Chem. Phys.* **1984**, *81*, 511.
(25) Hoover, W. *Phys. Rev. A* **1985**, *31*, 1695.
(26) Sikdar, D.; Katti, D. R.; Katti, K. S. *Langmuir* **2006**, *22*, 7738.
(27) Dorris, G. M.; Gray, D. G. *J. Colloid Interface Sci.* **1979**, *71*, 93.
(28) Conder, J. R.; Young, C. L. *Physicochemical measurement by gas chromatography*; Wiley: New York, 1979.
(29) Zeki, Y.; Saigh, A. L. *Polymer* **1999**, *40*, 3479.
(30) Tamargo-Martińez, K.; Villar-Rodil, S.; Paredes, J. I.; Martínez-Alonso, A.; Tascón, J. M. D.; Montes-Morán, M. A. *Macromolecules* **2003**, *36*, 8662.
(31) Montes-Morán, M. A.; Paredes, J. I.; Martínez-Alonso, A.; Tascón, J. M. D. *Macromolecules* **2002**, *35*, 5085.
(32) Yl-Mihniemi, P. P.; Heng, J. Y. Y.; Thielmann, F.; Williams, D. R. *Langmuir* **2008**, *24*, 9551.
(33) Castellano, M.; Conzatti, L.; Turturro, A.; Costa, G.; Busca, G. *J. Phys. Chem. B* **2007**, *111*, 4495.
(34) Flour, C. S.; Papirer, E. *J. Colloid Interface Sci.* **1983**, *91*, 69.
(35) Gutmann, V. *The donor-acceptor approach to molecular interactions*; Plenum: New York, 1978.
(36) Riddle, F. L.; Fowkes, F. M. *J. Am. Chem. Soc.* **1990**, *112*, 3259.

JP903448T